



ARTICLE

An Analysis of the Static and Dynamic Behavior of the Hydraulic Compensation System of a Multichannel Valve

Jikang Xu^{1,4}, Ruichuan Li^{1,2,*}, Yi Cheng², Yanchao Li³, Junru Yang³, Chenyu Feng⁴, Xinkai Ding² and Huazhong Zhang⁵

¹College of Transportation, Shandong University of Science and Technology, Qingdao, 266590, China

²School of Mechanical and Automotive Engineering, Qilu University of Technology, Jinan, 250353, China

³College of Mechanical and Electronic Engineering, Shandong University of Science and Technology, Qingdao, 266590, China

⁴Rizhao Haizhuo Hydraulic Co., Ltd., Rizhao, 276800, China

⁵Rizhao Polytechnic, Rizhao, 276800, China

*Corresponding Author: Ruichuan Li. Email: liruichuan@qlu.edu.cn

Received: 17 March 2022 Accepted: 29 June 2022

ABSTRACT

Electro-hydraulic proportional valve is the core control valve in many hydraulic systems used in agricultural and engineering machinery. To address the problem related to the large throttling losses and poor stability typically associated with these valves, here, the beneficial effects of a triangular groove structure on the related hydraulic response are studied. A mathematical model of the pressure compensation system based on the power-bond graph method is introduced, and the AMESim software is used to simulate its response. The results show that the triangular groove structure increases the jet angle and effectively compensates for the hydrodynamic force. The steady-state differential pressure at the valve port of the new pressure compensation structure was 0.65 MPa. Furthermore, experimental results show that the pressure difference at the main valve port is 0.73 MPa, and that the response time is less than 0.2 s. It is concluded that the new compensation structure has good pressure compensation response characteristics.

KEYWORDS

Electrohydraulic proportional valve; spool shape; pressure compensation; valve port differential pressure; response time

1 Introduction

Electrohydraulic proportional valve is the core control valve of hydraulic systems used in agricultural and engineering machinery. Its performance determines the reliability, stability, accuracy, and green energy savings of the entire hydraulic system. The performance of the electrohydraulic proportional valve directly affects the quality and efficiency of the entire operation [1–5]. The main drawback of electrohydraulic proportional valves is their poor pressure-compensation stability, which cannot meet the operational requirements of modern agricultural equipment in complex and dynamic field environments. This significantly hinders the development of high-end hydraulic components [6–10].



In recent years, electrohydraulic proportional valves and their pressure compensation technologies have rapidly developed. Rexroth and Eaton developed supporting technologies and products to satisfy various system requirements [11–15]. Some scholars have conducted in-depth research on pressure compensation valves to overcome traditional technical barriers. Xia et al. [16,17] analyzed the flow-pressure characteristics of a pressure compensation valve by considering the shape of the orifice as the research object. Milic et al. [18,19] analyzed the pressure compensation problem in an LUDV multiway valve and found that by reducing the spring stiffness of the pressure compensation valve, one can effectively increase the hydraulic buffer and improve the compensation effect. Grosbrink et al. [20,21] found that a system with pre-valve compensation has better speed regulation rigidity. They also studied the post-valve pressure compensation of a pressure compensation valve. However, these studies generally have insufficient innovation, and their structural design should be optimized. The pressure-compensation analyses focused on a certain parameter or variable, while the influence of other parameters and boundary conditions was not fully considered. The fretting response characteristics were poor and difficult to discern from the results. Moreover, there was a lack of objects for comparison, and it was impossible to define the technical level of the research results [22–26].

Therefore, in this study, an electrohydraulic proportional control valve was selected as the research object, and an advanced international reversing valve was selected as the reference object [27–31]. A mathematical model of the pressure compensation system was established using the power bond diagram method. The influence of the triangular groove shape of the valve core on the hydrodynamic response characteristics was analyzed using FLUENT. Simulation models of the pressure compensation system were built using AMESim software. A multiparameter simulation of the pressure compensation performance was conducted, and the parameters of the electrohydraulic proportional valve were optimized. Finally, the accuracy of the mathematical and simulation models of the pressure compensation system was verified experimentally.

2 Structural Composition and Working Principle of the Pressure Compensation System in the Electrohydraulic Proportional Valve

The pressure compensation system of an electrohydraulic proportional valve consists of a pressure compensation valve, spring, main valve, and various oil passages. The structure of the pressure compensation valve is illustrated in Fig. 1. The pressure compensation valve has a series-type pre-valve pressure compensation and is connected in series to the throttle port of the main valve to form a two-way speed-regulating valve. This ensures that the working pressure difference of the throttle valve does not change with load pressure fluctuation and realizes the independent function of the load. The pressure compensation valve has a separate modular interface design that can be directly inserted into the valve body without adjustment. The pressure compensation valve has the advantages of high-precision control, robust reliability, a reasonable and compact structure, and ease of maintenance.

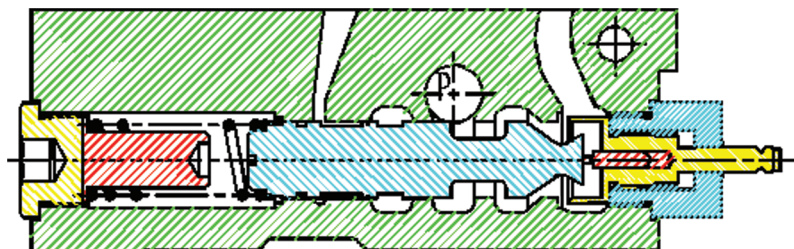


Figure 1: System structure of pressure compensation valve

The working principle of the pressure compensation system is that, when the valve is in operation, the hydraulic oil from the pressure port flows into the pressure compensation valve spool through the thin-walled hole to reach the installation valve seat. Subsequently, the spool is pushed to the left toward the position where the thin-walled hole is closed. The pressure compensation valve port and thin-walled hole opens, and a portion of the hydraulic oil input from the pressure port flows into the main valve cavity. Thus, the load pressure and main valve orifice exhibit a logical relationship. The remaining hydraulic oil flows through the thin-walled hole into the pressure cavity formed by the right end of the pressure compensation valve spool and the installed valve seat and participates in the stress of the pressure compensation valve spool. After a certain period, the pressure-compensating valve spool reaches a balanced state.

3 Mathematical Model and Characteristic Analysis of Pressure Compensation System

3.1 Mathematical Model of the Pressure Compensation System Based on Power-Bond Diagram

Fig. 2 shows the power-bond model of the pressure compensation system based on the working principle of the pressure compensation valve.

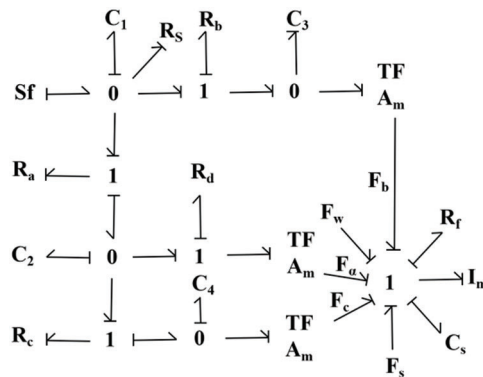


Figure 2: Power-bond diagram of the new pressure compensation system

A mathematical model is derived from the aforementioned power-bond diagram. The generalized displacement of element C and generalized momentum of element I in this system are considered as the state variables, which were set as X_i ($i = 1, 2, 3, 4, 5, 6$), expressed as follows:

$$\begin{cases} X_1 = \int q_1 dt & X_3 = \int q_3 dt & X_5 = \int F_m dt \\ X_2 = \int q_2 dt & X_4 = \int q_4 dt & X_6 = \int X'_m dt \end{cases} \quad (1)$$

which is

$$\begin{cases} \dot{X}_1 = q_1 = q_s - q_{Rs} - q_a - q_b & \dot{X}_3 = q_3 = q_b - q_{b3} & \dot{X}_5 = F_m = F_b + F_c - F_k - F_f - F_d - F_w - F_s \\ \dot{X}_2 = q_2 = q_a - q_c - q_a - q_d & \dot{X}_4 = q_4 = q_c - q_{c4} & \dot{X}_6 = \dot{X}'_m = \frac{1}{I_m} \int F_m dt \end{cases} \quad (2)$$

According to the above expressions, the state equation can be deduced as follows:

$$\dot{X}_1 = -\frac{1}{C_1} X_1 \left(\frac{1}{R_s} + \frac{1}{R_a} + \frac{1}{R_b} \right) + \frac{1}{C_2} \frac{1}{R_a} X_2 + \frac{1}{C_3} \frac{1}{R_b} X_3 + q_s, \quad (3)$$

$$\dot{X}_2 = -\frac{1}{C_2} X_2 \left(\frac{1}{R_a} + \frac{1}{R_c} \right) + \frac{1}{C_1} \frac{1}{R_a} X_1 + \frac{1}{C_4} \frac{1}{R_c} X_4 - \frac{A_m}{I_m} X_5, \quad (4)$$

$$\dot{X}_3 = -\frac{1}{C_3} \frac{1}{R_b} X_3 + \frac{1}{C_1} \frac{1}{R_b} X_1 - \frac{A_m}{I_m} X_5, \quad (5)$$

$$\dot{X}_4 = -\frac{1}{C_4} \frac{1}{R_c} X_4 + \frac{1}{C_2} \frac{1}{R_c} X_2 - \frac{A_m}{I_m} X_5, \quad (6)$$

$$\dot{X}_5 = -\frac{B_m}{I_m} X_5 + \frac{A_m}{C_3} X_3 + \frac{A_m}{C_4} X_4 - \frac{1}{C_5} X_6 - k \cdot x_0 - p_d \cdot A_m - F_w - F_s, \quad (7)$$

$$\dot{X}_6 = \frac{1}{I_m} X_5. \quad (8)$$

Each parameter in the formula is defined as follows:

Sf—Input source,

X_1 —Compressed fluid volume at pressure compensation valve inlet (m^3),

X_2 —Volume of oil compressed from pressure compensation valve port to main valve cavity (m^3),

X_3 —Volume of oil compressed from the small hole on the left side of the pressure compensation valve spool to the installation seat (m^3),

X_4 —Volume of oil compressed from the small hole on the right side of the pressure compensation valve spool to the installation seat (m^3),

X_5 —Pressure compensation valve spool momentum ($N \cdot s$),

X_6 —Pressure compensation valve spool displacement (m),

q_s —Pressure compensation valve inlet flow ($\frac{m^3}{s}$),

k —Pressure compensation valve spring rate ($7000 \frac{N}{m}$),

x_0 —Pressure compensation valve spring precompression ($0.013 m$),

X_m —Pressure compensation valve spool displacement (m),

I_m —Equivalent mass of pressure compensation valve spool ($0.15 kg$),

B_m —Pressure compensation valve spool viscous damping coefficient ($\frac{N \cdot s}{m}$),

A_m —Radial cross-sectional area of the pressure-compensating valve spool (m^2),

C_1 —Hydraulic pump outlet pipe connecting the block chamber liquid volume ($\frac{m^3}{P_a}$),

C_2 —Liquid volume from the pressure compensation valve to the main valve cavity oil passage ($\frac{m^3}{P_a}$),

C_3 —Liquid capacity of oil passage inside the pressure compensation valve spool ($\frac{m^3}{P_a}$),

C_4 —Equivalent oil passage fluid volume from small hole on right side of pressure compensation valve spool to installed valve seat ($\frac{m^3}{P_a}$),

C_5 —Pressure compensation valve spring compliance ($\frac{m}{N}$),

R_s —Pump leakage resistance $\left(\frac{kg}{m^4 \cdot s}\right)$,

R_a —Pressure compensation valve port liquid resistance $\left(\frac{kg}{m^4 \cdot s}\right)$,

R_b —Equivalent liquid resistance of small-hole oil passage in pressure compensation valve spool $\left(\frac{kg}{m^4 \cdot s}\right)$,

R_c —Equivalent oil passage liquid resistance from small hole on right side of pressure compensation valve spool to installed valve seat $\left(\frac{kg}{m^4 \cdot s}\right)$,

q_a —Flow through pressure compensation valve port $\left(\frac{m^3}{s}\right)$,

q_b —Flow from the small hole on the left side of the pressure compensation valve spool into the spool interior $\left(\frac{m^3}{s}\right)$,

q_c —Flow from the small hole on the right side of the pressure compensation valve spool into the spool interior $\left(\frac{m^3}{s}\right)$,

q_d —Flow through the main valve port $\left(\frac{m^3}{s}\right)$,

q_{b3} —Flow of oil from the small hole on the left side of the pressure compensation valve spool to the installed valve seat $\left(\frac{m^3}{s}\right)$,

q_{c4} —Flow of oil from the small hole on the right side of the pressure compensation valve spool to the installed valve seat $\left(\frac{m^3}{s}\right)$,

q_1 —Compressed oil flow at pressure compensation valve inlet $\left(\frac{m^3}{s}\right)$,

q_2 —Compressed oil flow from behind the pressure compensation valve port to the main valve cavity $\left(\frac{m^3}{s}\right)$,

q_3 —Compressed oil flow from the small hole on the left side of the pressure-compensating valve spool to the installed valve seat $\left(\frac{m^3}{s}\right)$,

q_4 —Compressed oil flow from the small hole on the right side of the pressure compensation valve spool to the installed valve seat $\left(\frac{m^3}{s}\right)$,

F_m —Resultant force driving the movement of the pressure compensation valve spool (N),

F_k —Spring force on the pressure compensation valve spool (N),

F_f —Frictional force during movement of pressure-compensating valve spool (N),

F_b —Axial force from the oil flowing from the left orifice of the pressure-compensating valve spool to the installed valve seat (N),

F_c —Axial force from the oil flowing from the small hole on the right side of the pressure-compensating valve spool to the installed valve seat (N),

F_d —Axial force from the oil in the spring chamber on the pressure-compensating valve spool (N),

F_w —Steady-state fluid power during movement of pressure compensation valve spool (N),

F_s —Transient fluid power from pressure compensation valve spool movement (N).

3.2 Theoretical Calculation of the Main Parameters of the Pressure Compensation System

(1) Calculation of the pressure compensation valve port liquid resistance.

The valve port of the pressure compensation valve is similar to the nonlinear liquid resistance and is expressed as follows:

$$R_a = \left(\pi C_f d_m X_6 \sqrt{\frac{2}{\rho}} \right)^{-1} \sqrt{\Delta p_{sa}}. \quad (9)$$

In the formula

C_f —Orifice flow coefficient (0.61),

d_m —Pressure compensation valve spool diameter (0.018 m),

X_6 —Valve opening (m),

ρ —Oil density $\left(900 \frac{kg}{m^3} \right)$.

(2) Calculation of the liquid guide during the process, from the small hole on the left side to the installed valve seat through the valve spool interior.

During this process, oil passes through thin-walled holes 1, 2, and 3. The liquid guide of the thin-walled holes is given as follows:

$$\frac{1}{R_{b1}} = C_f A_1 \sqrt{\frac{2C_1}{\rho}} \cdot X_1. \quad (10)$$

The following can be determined using the orifice flow formula: $q_b = KA_1 \sqrt{\Delta p_1}$, $q_b = KA_2 \Delta p_2$, $q_b = KA_3 \Delta p_3$, and $\Delta p_{sb} = \Delta p_1 + \Delta p_2 + \Delta p_3$. The liquid guide of elongated holes 2 and 3 can be expressed as $\frac{1}{R_{b2}} = \frac{q_b}{\Delta p_2 + \Delta p_3} = \frac{KA_2 A_3}{A_2 + A_3}$. Therefore,

$$\frac{1}{R_b} = \frac{1}{R_{b1} + R_{b2}} = \frac{1}{\left(C_f A_1 \sqrt{\frac{2C_1}{\rho}} \cdot X_1 \right)^{-1} + \frac{A_2 + A_3}{KA_2 A_3}}. \quad (11)$$

Each parameter in the formula is defined follows:

K —Throttle factor (0.48),

A_1 —Flow area of thin-walled orifice 1 (m^2),

A_2 —Flow area of elongated hole 2 (m^2),

A_3 —Flow area of elongated hole 3 (m^2).

Via calculation, it is known that

$$A_1 = \left\{ \left(\pi - \arccos \frac{r_1 - X_6}{r_1} \right) r_1^2 + (r_1 - X_6) \sqrt{2r_1 X_6 - X_6^2}, 0 \leq X_6 \leq 2r_1, \text{ other} \right. \quad (12)$$

$$A_2 = \pi r_2^2, \quad (13)$$

$$A_3 = \pi r_3^2. \quad (14)$$

Each parameter in the formula is defined as follows:

β —Central angle corresponding to the orifice opening (rad),

r_1 —Radius of thin-walled hole 1 (0.001375 m),

r_2 —Radius of elongated hole 2 (0.0011 m),

r_3 —Radius of elongated hole 3 (0.0015 m).

(3) Calculation of the liquid guide during the process, from the small hole on the right side to the installed valve seat through the valve spool interior.

Similar to (2), the liquid guide can be expressed as:

$$\frac{1}{R_c} = \frac{1}{\left(C_f A_4 \sqrt{\frac{2C_2}{\rho}} \cdot X_2 \right)^{-1} + \frac{A_5 + A_6}{KA_5 A_6}}, \quad (15)$$

$$A_4 = \left\{ r_4^2 \cdot \arccos \frac{r_4 - X_6 + 0.0022}{r_4} - (r_4 + 0.0022 - X_6) \sqrt{r_4^2 - (r_4 + 0.0022 - X_6)^2}, \right. \quad (16)$$

$$\left. 0.0022 < X_6 < 2r_4 + 0.0022, X_6 \geq 2r_4 + 0.0022, X_6 \leq 0.0022, \right.$$

$$A_5 = \pi r_5^2, \quad (17)$$

$$A_6 = \pi r_6^2. \quad (18)$$

Each parameter in the formula is defined as follows:

A_4 —Flow area of thin-walled orifice 4 (m^2),

A_5 —Flow area of elongated hole 5 (m^2),

A_6 —Flow area of elongated hole 6 (m^2),

γ —central angle corresponding to orifice opening (rad),

r_4 —Radius of thin-walled hole 4 (0.00165 m),

r_5 —Radius of elongated hole 5 (0.0011 m),

r_6 —Radius of elongated hole 6 (0.0015 m).

(4) Calculation of fluid power on the pressure compensation valve spool.

The steady-state flow force can be expressed using the valve port flow and flow rate formulas as follows:

$$F_w = 2C_v C_f A_a \Delta p_{sa} \cdot \cos \theta, \quad (19)$$

$$F_s = \rho L C_f \frac{dA_a}{dX_m} \cdot \sqrt{\frac{2}{\rho} \Delta p_{sa}} \cdot \dot{X}_m \quad (20)$$

Each parameter in the formula is defined as follows:

C_v —Orifice flow rate coefficient (0.98),

A_a —Orifice flow cross-sectional area (m^2),

θ —Throttle exit angle (1.1 rad),

L —pressure compensation valve damping length (0.006 m).

The pressure compensation valve orifice was of the triangular groove type. The two orifices are arranged symmetrically; therefore, the flow area is:

$$A_a = \begin{cases} 0, & X_6 \leq 0 \\ 2 \left[\frac{R_v^2 \theta_T}{2} - R_v \left(R_v - \frac{D_T}{L_T} X_6 \right) \sin \sin \frac{\theta_T}{2} \right] \cdot \cos \cos \alpha, & 0 < X_6 \\ < L_T \\ 2 \left[\frac{R_v^2 \theta_T}{2} - R_v (R_v - D_T) \sin \sin \frac{\theta_T}{2} \right] \cdot \cos \cos \alpha, & X_6 \geq L_T \end{cases} \quad (21)$$

$$\alpha = \arctan \frac{D_T}{L_T}. \quad (22)$$

Therefore,

$$F_w = \begin{cases} 4 C_v C_f \Delta p_{sa} \left[\frac{R_v^2 \theta_T}{2} - R_v \left(R_v - \frac{D_T}{L_T} X_6 \right) \sin \sin \frac{\theta_T}{2} \right] \cdot \cos \cos \alpha \cdot \cos \cos \theta, & 0 < X_6 \\ < L_T \\ 4 C_v C_f \Delta p_{sa} \left[\frac{R_v^2 \theta_T}{2} - R_v (R_v - D_T) \sin \sin \frac{\theta_T}{2} \right] \cdot \cos \cos \alpha \cdot \cos \cos \theta, & X_6 \geq L_T \end{cases} \quad (23)$$

$$F_s = \begin{cases} 2 \rho L C_f \frac{D_T R_v}{L_T} \sin \sin \frac{\theta_T}{2} \cos \cos \alpha \cdot \sqrt{\Delta p_{sa} \frac{2}{\rho}} \cdot \dot{X}_6, & 0 \leq X_6 \\ \leq L_T \\ 0, & \text{other.} \end{cases} \quad (24)$$

Each parameter in the formula is defined as follows:

R_v —Pressure compensation valve pool shoulder radius (0.009 m),

θ_T —Triangular groove corresponding to the central angle of the valve core (0.39 rad),

D_T —Radial height of triangular groove (0.001 m),

L_T —Axial length of triangular groove (0.0045 m),

α —Projection angle (rad).

4 Simulation Results and Analysis

4.1 Simulation of Hydrodynamic Change in the Valve Core

An improved valve core structure was designed, as shown in Fig. 3. The valve stem was shaped like a round table by reducing the diameter on one side. A triangular groove was circumscribed on each step on the same side. After part of the liquid flow is guided through the triangular groove, the flow direction changes; that is, a flow component along the closing direction of the valve core is generated. This part of the liquid flow impacts the positive direction liquid flow, such that the flow angle of the liquid at the outlet increases; therefore, the jet angle increases and the hydrodynamic force decreases. As the diameter of one

side of the valve stem decreases, the space on the side of the valve stem increases, enabling more liquid to be guided through the triangular groove, further reducing the hydraulic force.

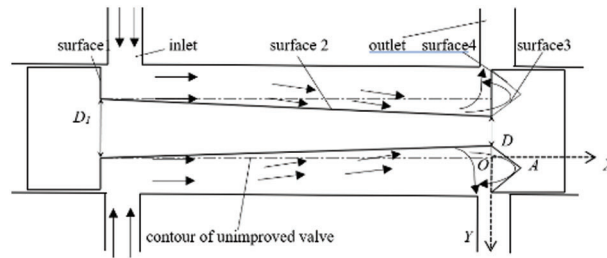


Figure 3: Improved valve core structure

Fig. 4 shows the jet angle distribution at the outlet of the original valve core. Fig. 5 shows the change in the jet angle when the bottom radius of the fixed triangular groove remains unchanged and the bottom depth increases. The comparison shows that the improved structure effectively increases the jet angle at the outlet, which increases with the groove bottom depth.

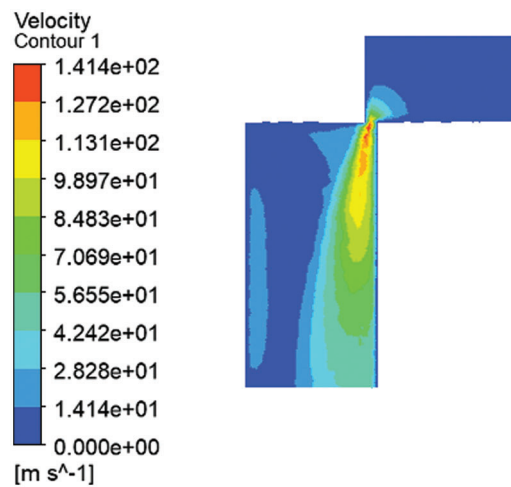


Figure 4: Original spool jet angle

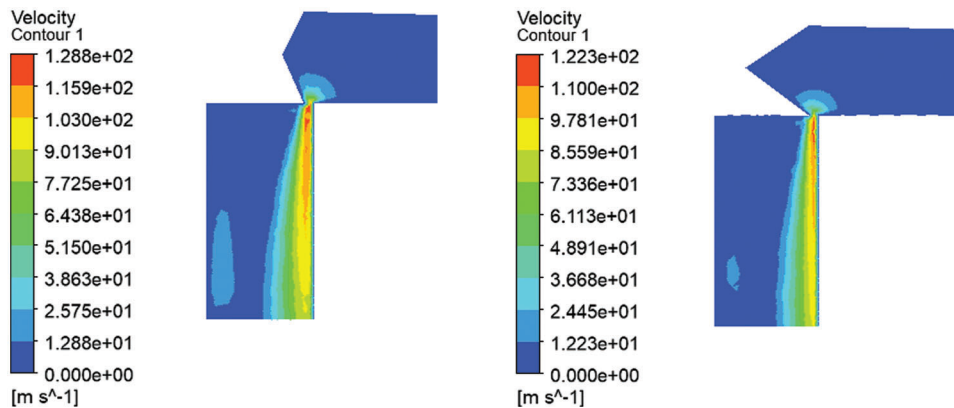


Figure 5: Jet angle with increasing groove bottom depth

Fig. 6 shows the change in the jet angle when the fixed groove bottom depth is unchanged and the groove bottom radius increases. The comparison shows that the jet angle increases with an increase in the groove bottom radius; however, the change range of the jet angle is small.

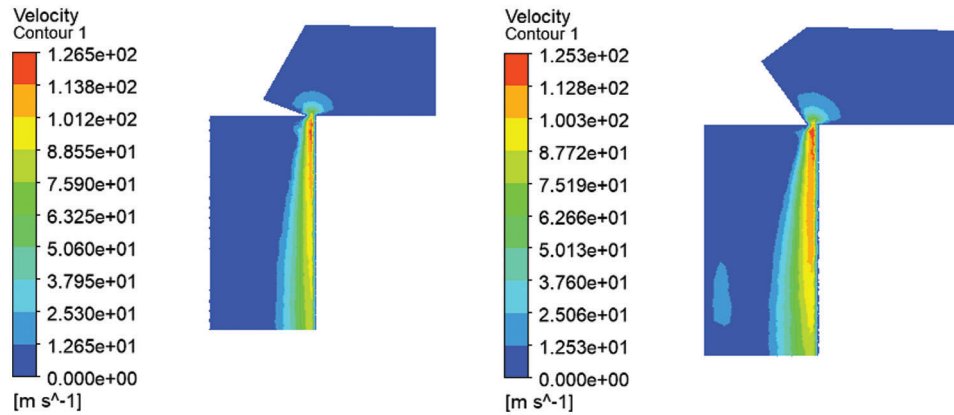


Figure 6: Jet angle with increasing groove bottom radius

The simulation results showed that the triangular groove structure can produce a flow component in the negative direction. This part of the liquid impacts the liquid flow in the positive direction, such that the flow angle of the liquid flow at the outlet increases; that is, the jet angle increases. The structure effectively compensates for the hydrodynamic force.

4.2 Simulation of the New Pressure Compensation System

The simulation model of the pressure compensation system in the electrohydraulic proportional control valve of agricultural and engineering machinery is shown in Fig. 7. To compare the simulation results of the advanced reversing valve and optimize the design of the electrohydraulic proportional control valve parameters, the influences of the spring preload, spring stiffness, and pressure compensation valve viscous damping coefficient on the pressure-compensation characteristics were studied.

The simulation parameters of the model are set as shown in Table 1.

(1) Influence of spring stiffness on compensation characteristics.

The spring stiffness comparison values were 20,000, 25,000, and 30,000 N/m. The simulation duration was set to 0.2 s. Fig. 8 shows the response curves for the different spring stiffness values.

From Fig. 8, it can be seen that as spring stiffness increases, the response speed of the output flow and differential pressure increases, peak time and peak value significantly decrease, system-adjustment time increases, stability decreases, and the steady-state output value slightly increases. For the displacement response of the pressure compensation valve spool, the peak value decreased as the spring stiffness increased; however, the maximum overshoot increased. When the spring stiffness was 30,000 N/m, the system adjustment time was shortest.

The spring preload affects the dynamic response and steady-state characteristics of the pressure compensation system of an electrohydraulic proportional valve. Within a certain range, the performance of the pressure compensation system can be improved by increasing spring stiffness. For the existing pressure compensation system model, the spring stiffness was set to 30,000 N/m.

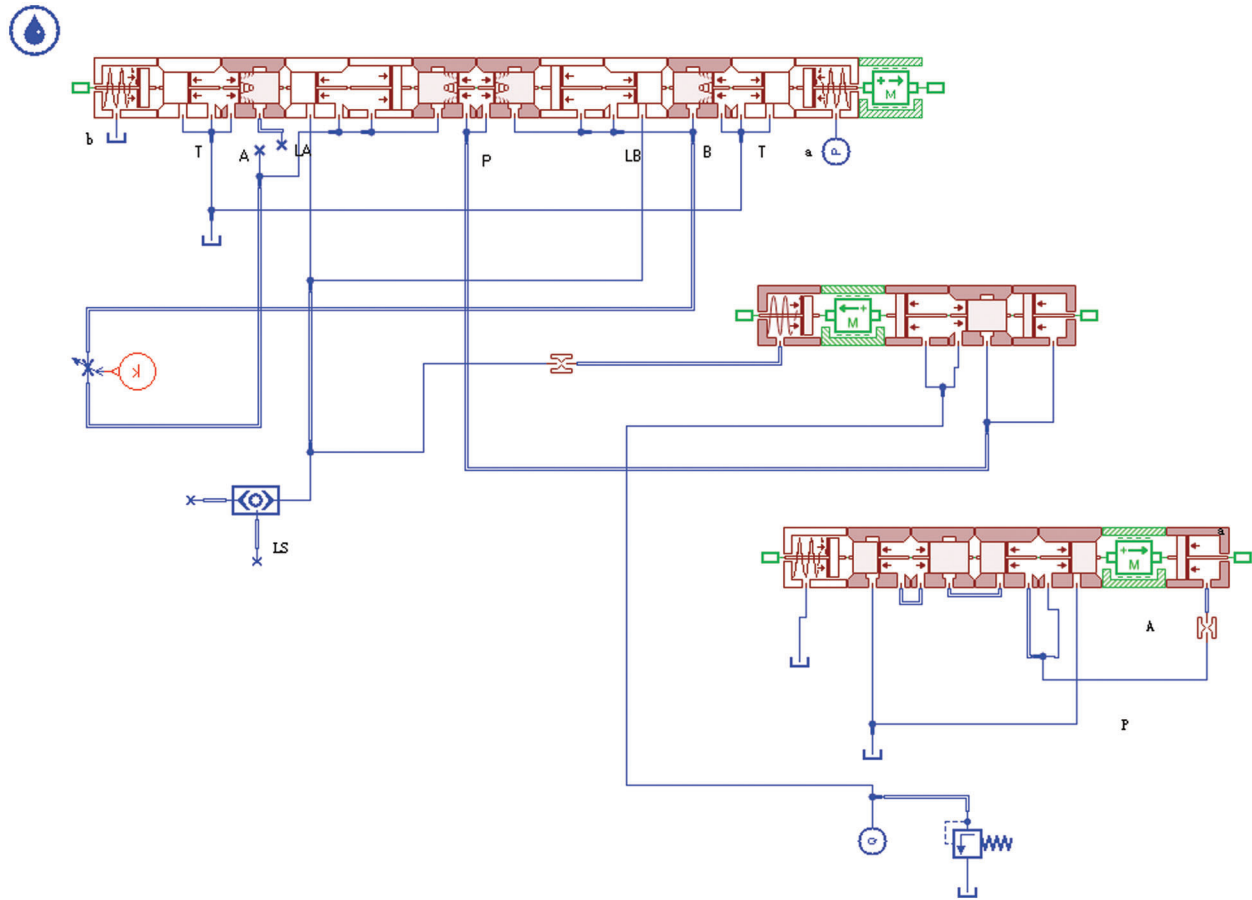


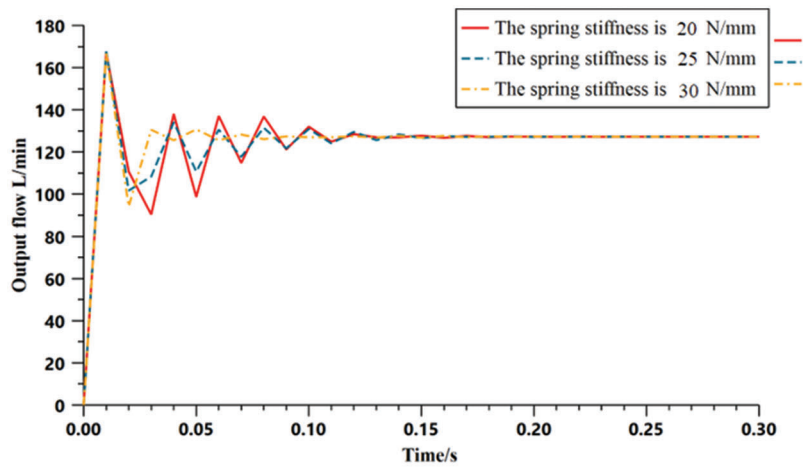
Figure 7: A simulation model of the new pressure compensation system

Table 1: Main parameters of the simulation model

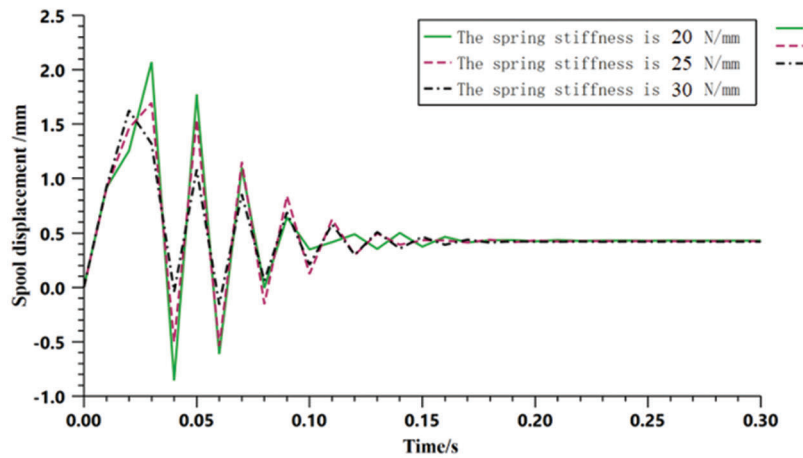
Serial number	Parameter	Numerical value	Unit
1	Pressure compensation valve spring rate	22	N/mm
2	Pressure compensation valve spring preload	454	N
3	Pressure compensation valve spool viscous damping coefficient	6.32	$N \cdot s/m$
4	Pressure compensation valve damping length	0.006	m
5	Equivalent mass of pressure compensation valve spool	0.2	kg
6	Control cavity orifice diameter	1.8	mm
7	Oil supply flow	200	L/min
8	Load pressure	29	MPa

(2) Influence of the spring preload on the compensation characteristics.

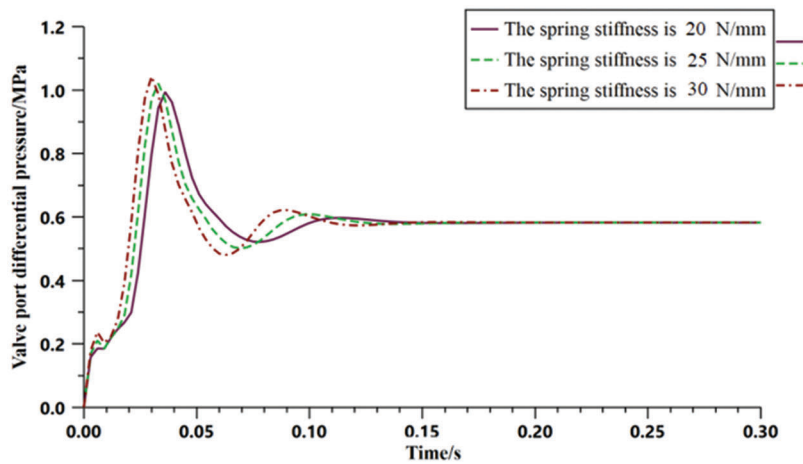
The comparison values of the spring preloads were 456, 471, and 486 N. The simulation duration was set as 0.2 s. The simulation results are shown in Fig. 9.



(a) Output flow-response curve

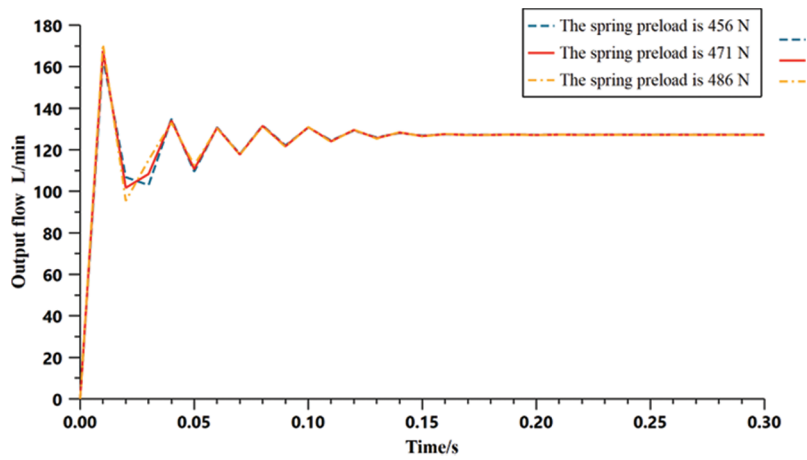


(b) Spool displacement-response curve for the pressure compensation valve

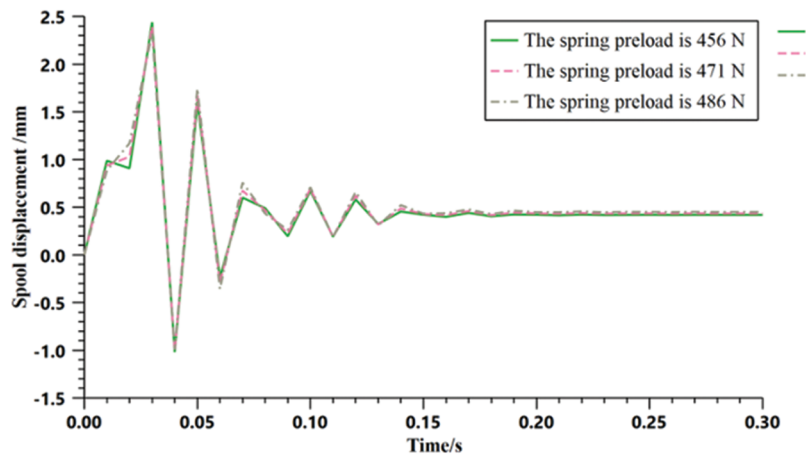


(c) Differential pressure-response curve of the main valve port

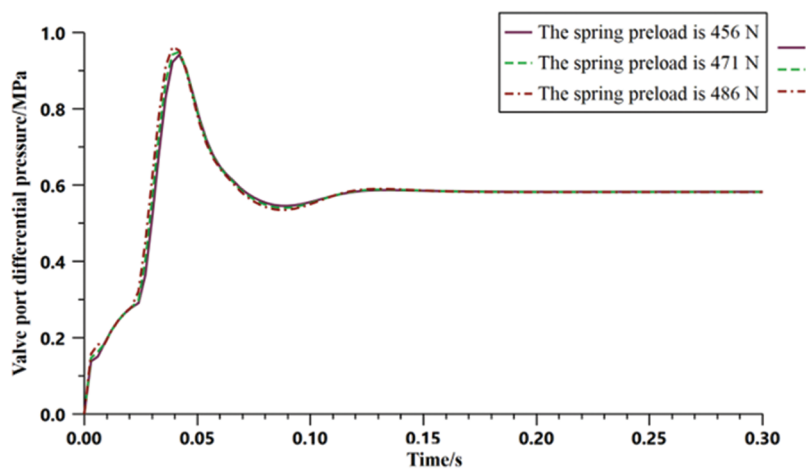
Figure 8: Response curves for different spring stiffness values



(a) Output flow-response curve.



(b) Spool displacement-response curve for the pressure compensation valve



(c) Differential pressure-response curve of the main valve port

Figure 9: Response curves for different spring preloads

Fig. 9 shows that the impact of the spring preload on the dynamic response and steady-state characteristics of the pressure compensation system of the electrohydraulic proportional valve. With the increase in spring preload of the pressure compensation valve, the maximum overshoot of the output flow and differential pressure significantly decreased, and the response stability slightly improved and the time to reach a steady-state decreased accordingly. The best response of the spool displacement was obtained at a spring preload of 471 N. When the preload was 486 N, the greatest fluctuation in spool displacement and longest system adjustment time were observed.

With the other parameters of the system remaining constant, increasing the spring preload of the pressure compensation valve within a certain range improves the stability of the pressure difference of the pressure compensation system, and the response characteristics of the output flow. It also improves the electrohydraulic pressure-compensation characteristic index of the proportional valve. For the current pressure compensation system model, a spring preload of 471 N is ideal.

(3) Influence of viscous friction coefficient on compensation characteristics.

The viscous friction coefficients in the dynamic simulation model were set as 0.5, 1.5, and 2.5 s·N/m, while other system parameters remained unchanged. The system pressure, load pressure, and simulation duration were 30, 29, and 0.2 s, respectively. The response curves for different viscous friction coefficients were obtained and are presented in Fig. 10.

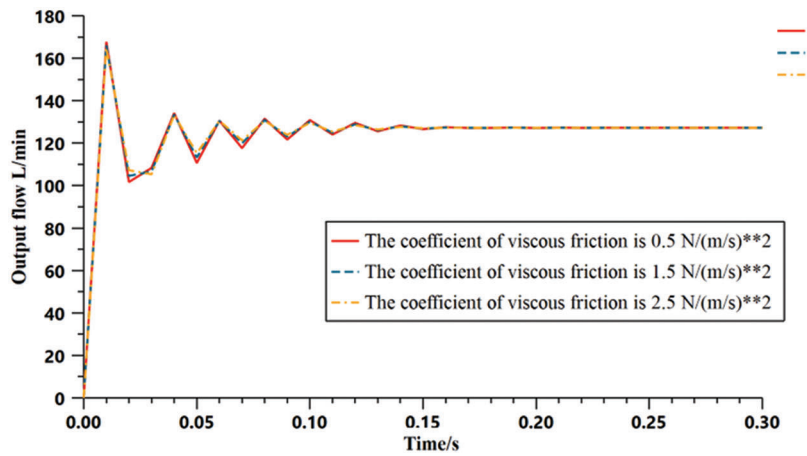
Fig. 10 shows that the change laws of the output flow-response curve and main valve port differential-pressure response curve are approximately the same. With the increase in the viscous friction coefficient, the peak value of the curve significantly increased, the peak time was slightly delayed, the maximum overshoot increased, and the system stability deteriorated. The time to reach a stable output state was the shortest at a viscous friction coefficient of $2.5 \frac{s \cdot N}{m}$. For the displacement-response curve of the pressure compensation valve spool, the peak values of the viscous friction coefficients were 0.5, 1.5, and 2.5 s·N/m. As the degree of fluctuation of the displacement decreased, the stability improved, and the system adjustment time decreased.

The magnitude of the viscous friction coefficient is a key factor affecting the dynamic response and steady-state characteristics of the pressure compensation system of the electrohydraulic proportional valve. Within a certain range, increasing or decreasing the viscous friction coefficient improved the performance of the pressure compensation system. Thus, in the design and manufacturing process, designers should pay special attention to the indirect control of the viscous friction coefficient. In the existing pressure compensation system model, the viscous friction coefficient was set to 2.5 s·N/m.

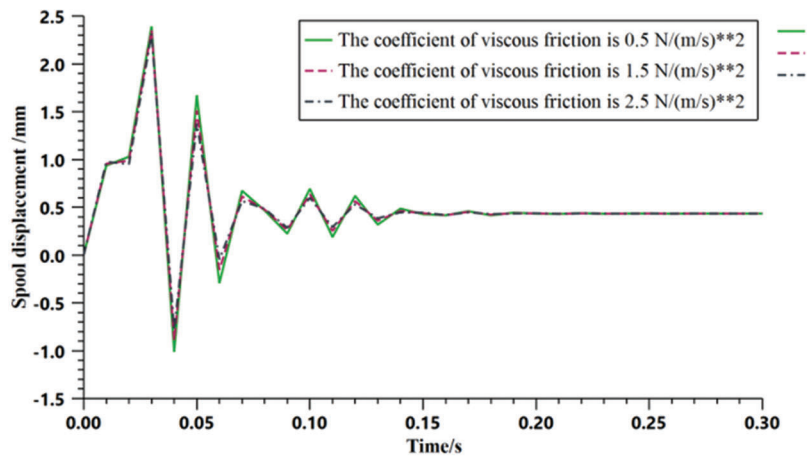
5 Experimental Verification

An electrohydraulic proportional-valve hydraulic system test platform was built to verify the accuracy of the mathematical model and simulation results of the pressure compensation system of the electrohydraulic proportional valve, as shown in Fig. 11. The test platform consisted of a measured electrohydraulic proportional valve, proportional electromagnet, load proportional relief valve, electrohydraulic proportional controller, and data acquisition system.

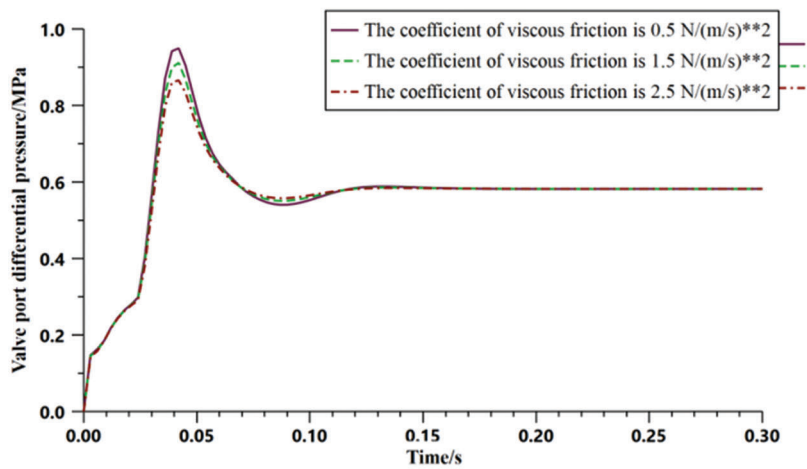
The system pressure was set to 30 MPa, and the loading pressure of the load-proportional relief valve was set to 29 MPa. A step signal with an amplitude of 8 V is applied to the proportional controller. The output flow response, spool displacement response, and main valve port differential pressure-response curves were obtained experimentally, as shown in Fig. 12.



(a) Output flow-response curve



(b) Spool displacement-response curve for the pressure compensation valve



(c) Differential pressure-response curve of the main valve port

Figure 10: Response curves for different viscous friction coefficients

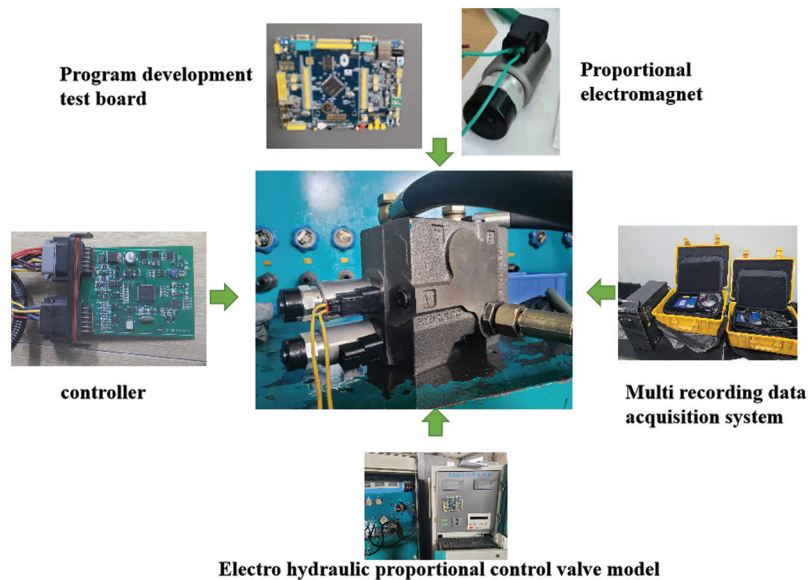
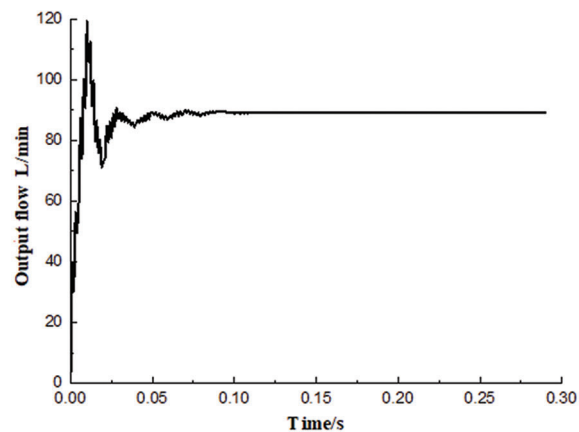


Figure 11: Electrohydraulic proportional valve hydraulic system test platform

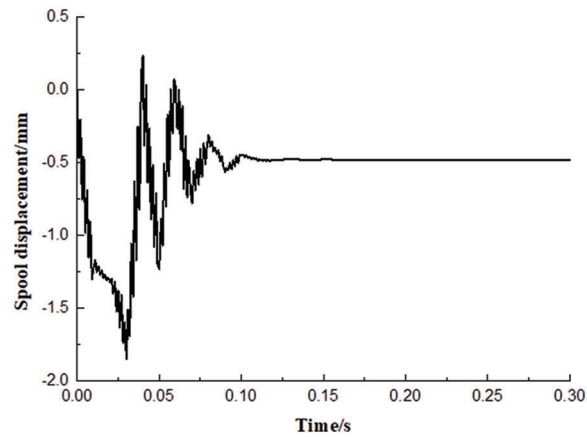
As shown in Fig. 12, the steady-state value of the output flow was 89.1 L/min, the maximum overshoot was approximately 33.3%, and the adjustment time was 0.12 s. The displacement-response time of the pressure compensation valve spool was 0.15 s, and the steady-state value was -0.49 mm. The response time of the pressure difference at the valve port was 0.2 s. The steady-state pressure difference was 0.73 MPa. When the main valve spool was at rest, the pressure difference between the two ends was 0.65 MPa. When the main valve port was open, the differential pressure changed dynamically with the response of the system pressure, causing output flow fluctuations. Thus, the trends in the changes shown in Figs. 12a and 12c are the same.

A comparison of the response curves of the test and simulation show that the simulation model built in this study accurately simulates the dynamic characteristics of the actual pressure compensation system.

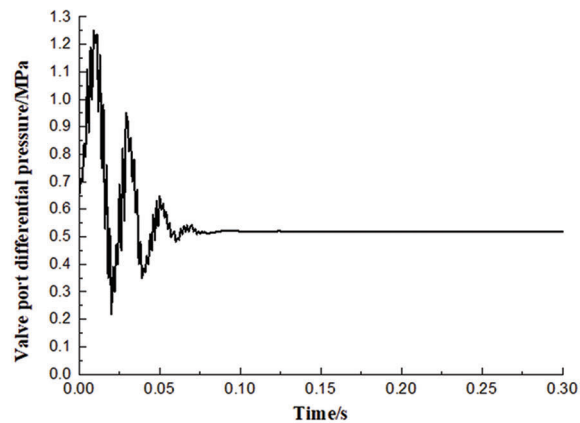


(a) Output flow-response curve

Figure 12: (Continued)



(b) Spool displacement-response curve for pressure compensation valve



(c) Differential pressure-response curve for main valve port

Figure 12: System response curves under step signal

6 Conclusion

- (1) The influence of the triangular groove shape of the valve core on the hydrodynamic response characteristics was analyzed using FLUENT software. The results showed that the triangular groove structure could produce a flow component in the negative direction. This part of the liquid flow reversely impacts the liquid flowing in the positive direction, thereby increasing the flow angle of the liquid at the outlet and jet angle. This structure effectively compensated for the hydrodynamic force and reduced pressure loss along the path.
- (2) The simulation models of the pressure compensation systems were built using AMESIM software. The influence of the pressure compensation valve spring preload, spring stiffness, and viscous damping coefficient on the pressure compensation characteristics was studied. The final spring preload, spring rate, and viscous damping coefficient were 471 N, 30000 N/m, and 2.5 s·N/m, respectively. A comparison of the load-step changes for the two systems showed that the response times of both systems were similar. The maximum fluctuations of the new pressure compensation system were 0.54 L/min, 0.017, and 0.006 MPa, with improved stability. In other words, its pressure compensation characteristics were better than those of the reverse valve.

- (3) A test platform was built to evaluate the electrohydraulic proportional valve. The results showed that the pressure difference at the main valve port was approximately 0.73 MPa, and the response time was approximately 0.2 s. The test and simulation curves were consistent, which verifies the accuracy of the mathematical and simulation models. An experimental analysis of different working conditions proved that the electrohydraulic proportional valve has good pressure-compensation performance and can replace similar products.

Acknowledgement: I would like to thank my tutor, R.L., for his support and guidance. I would also like to express my gratitude to my coworkers for their support and understanding, without which I would have never completed my research. I would also like to especially thank my family and friends, who listened to my frustrations and believed in me, sometimes more than I believed in myself.

Funding Statement: This research was funded by the 2020 Shandong Province Key Research and Development Programs (Major Technological Innovation Projects): Construction Machinery Integration Research and Application of Key Technologies for Intelligent Integration and Matching of Vehicle Assembly (2020CXGC011005), Large Tractor Hydraulic CVT Intelligent Continuously Variable Transmission Integration Research and Application (2020CXGC010806), and Development and Application of High-Horsepower High-Efficiency Intelligent Tractors (2021CXGC010812).

Conflicts of Interest: The authors declare that they have no conflicts of interest to report regarding the present study.

References

1. Liu, K., Gao, Y., Tu, Z. (2016). Energy saving potential of load sensing system with hydro-mechanical pressure compensation and independent metering. *International Journal of Fluid Power*, 17(3), 173–186. <https://doi.org/10.1080/14399776.2016.1185877>
2. Casoli, P., Riccò, L., Campanini, F., Lettini, A., Dolcin, C. (2015). Mathematical model of a hydraulic excavator for fuel consumption predictions. *Fluid Power Systems Technology*, 57236, V001T01A035. <https://doi.org/10.1115/FPMC2015-9566>
3. Pawanant, K., Leephakpreeda, T. (2019). Sequential control of multichannel on–off valves for linear flow characteristics via averaging pulse width modulation without flow meter: An application for pneumatic valves. *Journal of Dynamic Systems, Measurement, and Control*, 141(1), 011007. <https://doi.org/10.1115/1.4040969>
4. Bhushan, B. M., Yoon, J. Y., Griffith, L. G., Trumper, D. L. (2020). Flux-biased, energy-efficient electromagnetic micropumps utilizing bistable magnetic latching and energy-storage springs. *IEEE/ASME Transactions on Mechatronics*, 26(5), 2362–2372. <https://doi.org/10.1109/TMECH.2020.3038885>
5. Hsieh, C. T., Lai, C. P. (2019). Nonlinear dynamic analysis and control of a hydraulic press electro-hydraulic servo system. *Journal of Low Frequency Noise Vibration and Active Control*, 38(3), 1594–1606. <https://doi.org/10.1177/1461348418813021>
6. Dindorf, R., Wos, P. (2019). Force and position control of the integrated electro-hydraulic servo-drive. *2019 20th International Carpathian Control Conference (ICCC)*, pp. 277–282. Poland.
7. Kumar, S., Tewari, V. K., Bharti, C. K., Ranjan, A. (2021). Modeling, simulation and experimental validation of flow rate of electro-hydraulic hitch control valve of agricultural tractor. *Flow Measurement and Instrumentation*, 82, 102070. <https://doi.org/10.1016/j.flowmeasinst.2021.102070>
8. Essa, M. E. S. M., Aboelela, M. A., Hassan, M. M., Abdraboo, S. M. (2019). Fractional order fuzzy logic position and force control of experimental electro-hydraulic servo system. *2019 8th International Conference on Modern Circuits and Systems Technologies (MOCASST)*, pp. 1–4. Thessaloniki, Greece.
9. Ko, Y. R., Kim, T. H. (2020). Feedforward plus feedback control of an electro-hydraulic valve system using a proportional control valve. *Actuators*, 9(2), 45. <https://doi.org/10.3390/act9020045>

10. Tic, V., Rotovnik, A., Lovrec, D. (2021). Impact of proportional valves' differences to ensure uniform motion of hydraulic motors. *International Journal of Simulation Modelling*, 20(1), 52–63. <https://doi.org/10.2507/IJSIMM>
11. Wos, P., Dindorf, R. (2019). Self-tuning controllers based on polynomial methods for electro-hydraulic servo drive. *10th International Conference on Applied Mechanics*, vol. 2077, pp. 020063. Poland.
12. Thomas, A. T., Parameshwaran, R., Sathiyavathi, S., Starbino, A. V. (2021). Practical profile tracking for a hydraulic press using sliding mode controller. *Proceedings of the Institution of Mechanical Engineers Part C: Journal of Mechanical Engineering Science*, 236(2), 1202–1213.
13. Hagen, D., Padovani, D., Choux, M. (2020). A comparison study of a novel self-contained electro-hydraulic cylinder versus a conventional valve-controlled actuator–Part 1: Motion control. *Actuators*, 8(4), 79. <https://doi.org/10.3390/act8040079>
14. Thangavel, S., Maheswari, C., Priyanka, E. B., Iyanka, E. B. (2021). Dynamic modeling and control analysis of industrial electromechanical servo positioning system using machine learning technique. *Journal of Testing and Evaluation*, 49(4), 2425–2440. <https://doi.org/10.1520/JTE20200159>
15. Lisowski, E., Filo, G. (2017). Analysis of a proportional control valve flow coefficient with the usage of a CFD method. *Flow Measurement and Instrumentation*, 53(B), 269–278. <https://doi.org/10.1016/j.flowmeasinst.2016.12.009>
16. Xia, Q. C. (2013). *Research on static and dynamic characteristics of a series of load-sensitive proportional multi-way valve (Master Thesis)*. Yanshan University, China.
17. Zhao, R. H., Liao, Y. Y., Lian, Z. S., Li, R. Z., Guo, Y. C. (2021). Research on the performance of a novel electro-hydraulic proportional directional valve with position-feedback groove. *Proceedings of the Institution of Mechanical Engineers, Part E: Journal of Process Mechanical Engineering*, 235(6), 1930–1944. <https://doi.org/10.1177/09544089211024424>
18. Milic, V., Situm, Z., Essert, M. (2010). Robust H-infinity position control synthesis of an electro-hydraulic servo system. *ISA Transactions*, 38(3), 1594–1606.
19. Yi, Y., Hu, Y. P., Mo, H. (2018). Research on steady characteristics of F- π bridge electrohydraulic proportional pressure reducing valve. *International Journal of Fluid Machinery and Systems*. 11(2), 154–162.
20. Grosbrink, B., Harms, H. (2009). Control concept for an advanced load-sensing system. *Proceedings of the 7th International Conference on Fluid Power Transmission and Control*, Hangzhou, China.
21. Axin, M., Eriksson, B., Palmberg, J. O., Krus, P. (2011). Dynamic analysis of single pump, flow controlled mobile systems. *The Twelfth Scandinavian International Conference on Fluid Power*, pp. 223–238. Tampere, Finland.
22. Axin, M., Eriksson, B., Palmberg, J. O. (2009). Energy efficient load adapting system without load sensing: Design and evaluation. *The 11th Scandinavian International Conference on Fluid Power*, pp. 58–73. Linköping, Sweden.
23. Wu, W., Wei, C. H., Zhou, J. J., Hu, J. B., Yuan, S. H. (2021). Numerical and experimental nonlinear dynamics of a proportional pressure-regulating valve. *Nonlinear Dynamics*, 103(2), 1415–1425. <https://doi.org/10.1007/s11071-020-06125-0>
24. Mannesmann, R. (2019). Mobile hydraulics and electronics. RE6400/08.92.
25. Zhao, J. W. (2013). *Research on shunt control of multi-actuator load sensing system (Master Thesis)*. Yanshan University, China.
26. Wang, B. L. (2009). Application of load sensing and pressure compensation technology in aerial hydraulic system. *China Ship Repair*, 22(4), 61–62.
27. Sun, H. L., Li, R. C., Xu, J. K., Xu, F. N., Zhang, B. et al. (2021). Fractional modeling and characteristic analysis of hydro-pneumatic suspension for construction vehicles. *Processes*, 9(8), 1414. <https://doi.org/10.3390/pr9081414>
28. Sun, H. L., Li, R. C., Huang, M. M., Li, Z., Xu, J. K. (2021). Numerical simulations of the influence of inert gases (N₂/CO₂) on combustion characteristics of laminar-premixed biosyngas flame. *ACS Omega*, 2(6), 14585–14597. <https://doi.org/10.1021/acsomega.1c01729>
29. Xu, J. K., Li, R. C., Li, Y. C., Zhang, Y. S., Sun, H. L. et al. (2021). Research on variable-universe fuzzy control technology of an electro-hydraulic hitch system. *Processes*, 9(11), 1920. <https://doi.org/10.3390/pr9111920>

30. Li, R. C., Ding, X. K., Lin, J. H., Chi, F., Xu, J. K. et al. (2021). Study on the influence of triangular groove structure on steady-state flow force compensation characteristics. *Applied Sciences*, 11(23), 11354. <https://doi.org/10.3390/app112311354>
31. Al-Zughaibi, A., Xue, Y. Q., Grosvenor, R., Okon, A. (2019). Design and investigation of pole assignment controller for driving nonlinear electro hydraulic actuator with new active suspension system model. *Proceedings of the Institution of Mechanical Engineers, Part D: Journal of Automobile Engineering*, 233(13), 3460–3479.